Articles

Submicron Multiphoton Free-Form Fabrication of Proteins and Polymers: Studies of Reaction Efficiencies and Applications in Sustained Release

Jonathan D. Pitts,[†] Paul J. Campagnola,[*,‡] Gary A. Epling,[§] and Steven L. Goodman[⊥]

Center for Biomaterials, The University of Connecticut Health Center, Farmington, Connecticut 06030, Department of Physiology and Center for Biomedical Imaging Technology, The University of Connecticut Health Center, Farmington, Connecticut 06030, Department of Chemistry, The University of Connecticut, Storrs, Connecticut 06269, and Department of Physiology and Center for Biomaterials, The University of Connecticut Health Center, Farmington, Connecticut 06030

Received June 29, 1999; Revised Manuscript Received November 16, 1999

ABSTRACT: Nonlinear multiphoton photo-cross-linking and photopolymerization of proteins and polymers in solution have been used to direct the three-dimensional assembly of micron scale objects. Two aspects of fabricated proteinatious matrixes are examined in this paper: the efficiency of protein photopolymerization and the application of fabricated matrixes as sustained release devices. The efficiency of photoactivated cross-linking of the proteins bovine serum albumin and fibrinogen, using rose bengal, have been determined and found to vary with photosensitizer concentration. This concentration dependence suggests that the mechanism for protein cross-linking is a direct hydrogen transfer between an amino acid residue of the protein and the dye molecule itself. A comparison of the surface structure of single and multiple protein oligomers is undertaken and shown to vary significantly depending on fabrication materials. Alkaline phosphatase bioactivity, upon entrapment in a protein structure, is maintained. The properties of fabricated protein matrixes as sustained release devices is also examined. The rates of diffusion of fluorescently labeled dextrans (10 and 40 kDa) from an optically fabricated BSA matrix vary with molecular weight and are linear with cross-link density. The half-life of release of 10 kDa dextran-TMR from a BSA micron scale structure is less than or equal to 6 min while 40 kDa dextran-TMR half-life of release is 25 min. Finally, rhodamine 610, a typical drug size molecule, was entrapped in an acrylamide structure, and its release is found to be diffusion-limited with half-lives of 10−31 min, depending on cross-link density.

Introduction

The development of micro- and nanofabrication techniques has shown particular promise in the engineering of micro-electromechanical systems (MEMS), biomimetics, and microfluidic devices.[1,2] Most fabrication techniques currently employed are inherently two-dimensional and involve complicated stamping, chemical etching, or methods that are combinations of both. Microcontact printing (μCP) has been widely used to fabricate structures on the micrometer to submicrometer scales.[1−4] Microcontact printing involves the casting of an elastomer, typically poly(dimethylsiloxane) (PDMS), onto a master substrate produced by photolithography. The master and the elastomer are then separated after curing, resulting in a stamp that is then "inked" and pressed onto a metal-coated silicon substrate. This method has been utilized for fabrication of many two-dimensional structures, as well as being used in combination with chemical etching to extend the process to microlithography.[3] Additionally, μCP has been used to control the position and distribution of cells on micron scale features.[2] Although μCP has significant potential in microfabrication, there are several associated drawbacks limiting its general applicability. The first is that since μCP is inherently two-dimensional, it has not proven particularly useful for creating complex features in three dimensions. The second is that the process is limited to certain materials for stamps and "inks", typically PDMS and thiols, respectively. Although μCP has had limited success with other materials, such as proteins and antibodies,[5] the technique does not have generality in terms of available chemistries. Finally the process is multistepped, involving careful preparation of the master, stamp, ink, and substrates.

Photolithography, another well-established method of fabrication, has been the industry standard for semiconductor fabrication. Still, photolithography has many of the same limitations of μCP, including limited and difficult chemistries and that expensive masks and substrates are required. Moreover, the scale of fabrication is most often in the micron to submicron range with a practical resolution limit of approximately 200 nm,

[†] Center for Biomaterials.
[‡] Department of Physiology and Center for Biomedical Imaging Technology.
[§] The University of Connecticut.
[⊥] Department of Physiology and Center for Biomaterials.

10.1021/ma9910437 CCC: $19.00
Published on Web 02/05/2000

and the process is essentially two-dimensional. Despite these limitations, both μCP and photolithographic techniques have proven useful in the engineering of microdevices, array chips, and "lab on a chip" devices.[1−4,6]

Recently, a new experimental approach for the free-form fabrication of synthetic polymers and proteins that allows for submicron feature sizes and complete three-dimensional (3D) freedom has been developed.[7] This new technique relies on a nonlinear optical photopolymerization process to spatially control fabrication. Fabrication is performed directly within a solution containing a photoinitiator, a co-initiator, and monomer substrates. To achieve 3D spatial resolution, a femtosecond laser is focused into a photopolymerizable or cross-linkable material, and photoactivation occurs via a multiphoton process. Since high photon densities are required to initiate the multiphoton process, polymerization and cross-linking reactions are confined to the focal point. The three-dimensionality is inherent in the ability not only to scan the laser in the *x* and *y* direction but also to change the focal plane (*z*) without overwriting existing features. This new method is a more direct route for fabrication than either microcontact printing or photolithography and stands to be much more general in terms of the available chemistries. Although in its infancy, this new method of free-form nanofabrication shows particular promise, circumventing the size and dimensionality limitations of previous free-form techniques. At its present stage of development, the size limitations are comparable to photolithography, i.e., 250 nm, but the addition of a third dimension makes this a truly novel technique.

One of the first examples of photoactivated, nonlinear 3D microfabrication was by Maruo et al.[8] where fabrication of micron scale helixes, made in a urethane acrylic resin, was accomplished. Witzgall et al.[9] used a similar multiphoton technique to fabricate 3D cylinder shaped features in negative photoresist materials. This technique requires a developing step to wash away any unexposed resist solution, leaving the light exposed area behind. Most recently, Cumpston et al. fabricated microcantilevers, photonic band gap structures, and a tapered waveguide structure from a resin containing photoactivators designed to possess large two-photon absorption cross sections.[10]

To the best of our knowledge, this methodology, so far, has been limited to synthetic polymer resins. Recently, our group has demonstrated multiphoton fabrication with proteins[7] and acrylamide[11] directly from solution. In these studies fabrication in two and three dimensions is accomplished with synthetics and proteins, and protein retained bioactivity is shown. In the current paper we extend this work to fabrication with other synthetic polymers, study the efficiency of protein photo-cross-linking, and examine the use of fabricated matrixes as sustained release devices. Specifically, we examine two- and three-photon fabrication of the synthetic organic polymer trimethylolpropane triacrylate and two proteins, bovine serum albumin (BSA) and fibrinogen. It is shown that free-form 3D fabrication of these materials is achieved with the same submicron spatial resolution and free-form abilities that are present in our previous studies.[7,11]

This paper examines two aspects of the photopolymerization of BSA and fibrinogen. The first is the efficiency of fabrication of BSA and fibrinogen as a function of photoinitiator concentration. This study

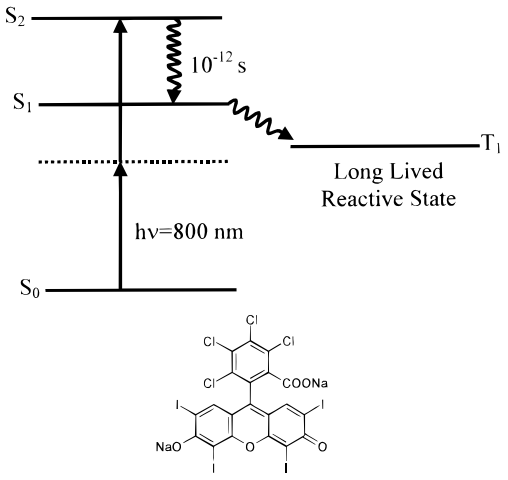

Figure 1. Molecular structure of rose bengal and energy level diagram for two-photon excitation. Two 800 nm photons are simultaneously absorbed to reach the S_2 electronic state. This excitation proceeds through a virtual or nonstationary state. The S_2 state rapidly decays nonradiatively to the S_1 electronic state. Finally the S_1 population interconverts to the final reactive T_1 state.

represents, to the best of our knowledge, the first two-photon photoinitiated cross-linking of proteins directly from solution. We then continue our study by applying these optimized fabrication parameters to produce micron-scale structures that will entrap compounds during fabrication and then release these compounds in a sustained fashion. As a model system, we examine the rates of diffusion of fluorescently labeled polysaccharides as a function of the fabricated structure composition and density. Observations on the surface characteristics of fabricated proteins, synthetic polymers, and hybrid structures are made, leading to conclusions on the rate of sustained release as well as the mechanism of polymerization/cross-linking. Finally, we study the rate of diffusion of rhodamine 610, a drug size molecule, out of a micron-scale slab of polyacrylamide.

Physical Background of Multiphoton Polymerization. In the data presented here, photopolymerization occurs via a multiphoton process, where excitation of a photoinitiator proceeds through one or more virtual states. The simultaneous absorption probability through a virtual state(s) is given by P^n/τ^{n-1}, where P is the laser pulse energy, n is the number of photons to be absorbed, and τ is the laser pulse width. It is this dependence on τ that necessitates the use of ultrafast lasers for multiphoton polymerization. The use of femtosecond or picosecond lasers has the added advantage of keeping the average laser power low, which avoids photodamage in biological samples.

Multiphoton excitation proceeding through a virtual, or nonstationary, state was predicted in the early part of this century by Goppert-Mayer.[12] Figure 1 shows a diagram that describes the two-photon excitation for the photoinitiator rose bengal (RB). The S_1 state may be reached via a single-photon excitation of 550 nm or in a multiphoton approach via two 800 nm photons. Multiphoton excitation at 800 nm actually reaches the S_2 electronic state by proceeding through a virtual state; this state subsequently decays nonradiatively (10^{-12} s) with near unit efficiency to the S_1 state. Interconversion of the S_1 population to the long-lived (1 ms) T_1 electronic state, having an efficiency of >98%, becomes the final

reactive state. As shown below, the formation of a long-lived triplet state can initiates a free-radical polymerization mechanism in the presence of a co-initiator (CI).[13−16]

$$\begin{aligned} \mathrm{RB} + 2h\nu &\rightarrow [\mathrm{RB}]_{\mathrm{triplet}} \\ [\mathrm{RB}]_{\mathrm{triplet}} + \mathrm{CI} &\rightarrow [\mathrm{RB}]^{\bullet -} + \mathrm{CI}^{\bullet +} \\ \mathrm{CI}^{\bullet +} + \mathrm{monomer} &\rightarrow \mathrm{R}^{\bullet} \\ \mathrm{R}^{\bullet} + (\mathrm{monomer})_{n-1} &\rightarrow \mathrm{R}-(\mathrm{monomer})_{n}^{\bullet} \end{aligned} \qquad (1)$$

Using a multiphoton approach for submicron photopolymerization has several advantages. First, polymerization is confined to only the focal volume. This is because simultaneous absorption of multiple photons requires a very high photon flux, which is only present at the point of focus. This allows for precise spatial fabrication in solution by avoiding nonspecific polymerization outside of the focal volume. Second, there is reduced photobleaching of the photoactivatable dyes used for polymerization. Third, there is no linear near-IR absorption out of the plane in most biomacromolecule samples.[17] And finally, the longer wavelength light provides a greater penetration depth, allowing for fabrication of objects below the surface of biological samples and many other materials.

Experimental Section

Details of the experimental setup are given elsewhere.[7,11] Briefly, a femtosecond near-infrared titanium sapphire oscillator (Coherent 900-F) pumped by an argon ion laser (Coherent Innova 310) is coupled into an upright laser scanning confocal microscope (Biorad MRC600) equipped with a 0.75 numerical aperture (NA) objective (Zeiss 20× Fluar). The laser, operating at 76 MHz, has a pulse width of 100 fs and is tunable between 700 and 1000 nm with a bandwidth of 10 nm (fwhm). In our present configuration, the laser scanning microscope is equipped with $x-y$ galvo scanning mirrors that can perform line, raster, and point scans. The laser dwell time is 1.6 μs/pixel, corresponding to approximately 50 laser pulses per pixel. All fabrication takes place, directly from solution, on glass microscope slides that have been previously washed in acetone for 20 min to remove any unwanted residue present on the slide that could potentially affect polymerization. The average laser power arriving at the fabrication zone is kept constant at 120 mW, independent of wavelength, allowing for a direct comparison of efficiencies of polymerization between samples and between separate experiments.

Fabricated features are analyzed by light microscopy and scanning electron microscopy (SEM). Transmitted light microscopy is used for actively observing structures during fabrication, as well as for optimizing fabrication parameters such as position on the substrate and selection of the focal plane. The confocal microscope is also equipped to detect epi-illuminated fluorescence, which is used to monitor diffusion of fluorescently labeled compounds, as well as to image constructs that have fluorophores either entrapped or internally cross-linked. Finally, SEM is used to image structures postfabrication, providing a method of measuring feature sizes that is not diffraction limited. Postfabrication, all protein samples are fixed in a 2% gluteraldehyde/HEPES solution for 30 min and dehydrated through increasing serial ethanol concentrations (25%, 50%, 75%, 95%, 2 × 100%) for 3 min per wash. The samples were then placed in hexamethyldisilazane, a low surface tension liquid, for 6 min and finally allowed to air-dry.[18] Samples are then mounted for SEM and sputter-coated with 10 nm of Au/Pd. Synthetic samples were simply washed with appropriate solvents (i.e., acetone, water, or methanol as determined by bulk polymer reactivity with each) and allowed to air-dry.

Norland Optical Adhesive 83H (Norland Products), trimethylolpropane triacrylate (Aldrich), triethanolamine (Aldrich), rose bengal (Sigma), 9-fluorenone-2-carboxylic acid (Aldrich), bovine serum albumin (Calbiochem), fibrinogen (Sigma), alkaline phosphatase (Sigma), ELF-97 phosphatase substrate (Molecular Probes), 10 and 40 kDa dextran−tetramethylrhodamine (Molecular Probes), and rhodamine 610 (Exciton) were all used without further purification.

Results and Discussion

Photochemical Fabrication Systems. The substrates utilized in the following experiments can be separated into classes of synthetics and proteins. In the present study two synthetic polymers are used. The first is a commercially available proprietary polyurethane liquid resin (Norland Optical Adhesive 83H) consisting of a prepolymer and a UV photoactivator that upon exposure to 800 nm light undergoes a simultaneous two-photon absorption and subsequent polymerization. The second synthetic compound is trimethylolpropane triacrylate (TMPTA) which in the presence of rose bengal and the co-initiator triethanolamine (TEA) (0.1 M) can be polymerized by two-photon excitation of 800 nm light. The most likely mechanism for TMPTA polymerization[19] is an intermolecular electron transfer from the TEA to the excited dye, forming a stable TEA radical cation that initiates polymerization by removal of an electron from the TMPTA monomer (mechanism 1, where TEA acts as CI). Although this is a more complicated set of two, two-body reactions, the polymerization kinetics are improved, over simple dye radical anion initiated polymerization, because the TEA radical cation is much longer lived than the RB triplet state (∼1 ms) itself. An analogous mechanism can be used for the polymerization of TMPTA that utilizes a three-photon activation process with 9-fluorenone-2-carboxylic acid (referred to as 9F2C) as the photoinitiator. This three-photon process (absorption at 780 nm) has the added advantage of a smaller interaction volume,[20] leading to a smaller fabrication zone compared to the two-photon absorption.

The second class studied here are protein biopolymers. In the following study two different size proteins were chosen, bovine serum albumin (BSA MW = 66 kg/mol) and fibrinogen (MW = 340 kg/mol). We have found that BSA and fibrinogen may be photo-cross-linked with only a photoinitiator; i.e., TEA is not required to facilitate cross-linking and in fact appears to act as an inhibitor.[7] This phenomenon may rely on the protein itself to fulfill the role of co-initiator as well as cross-linkable species, or, as will be shown below, a different reaction mechanism, compared to mechanism 1, is followed for the cross-linking of proteins. Protein cross-linking without a co-initiator is believed to occur in one of two ways.[21−25] These two photooxidation mechanisms involve excitation of a photoinitiator to the T_1 state, where the excited photoinitiator can then either transfer energy to the ground state triplet molecular oxygen, generating singlet molecular oxygen, or abstract hydrogen directly from a protein molecule. The singlet oxygen mechanism continues by reacting with an oxidizable amino acid residue of the protein. This irreversible mechanism generates an electron-deficient protein that may react with another protein's amino acid residue and form a covalent bond.[24] It is unclear exactly what the reactive species is, but it must involve residues at or near the protein surface. It has also been shown that protein cross-linking generally favors residues containing olefins, dienes, aromatics, and heterocycle groups

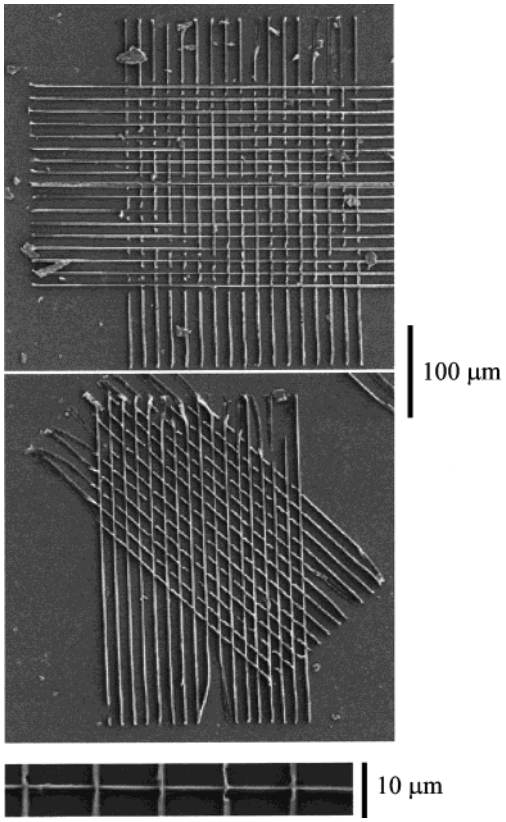

Figure 2. SEM micrographs of two lattice-like structures made by free-form optical polymerization of trimethylolpropane triacrylate (TMPTA). 9F2C (1×10^{-4} M) is used as the photoinitiator, TEA (0.1 M) is the co-initiator, and each line is fabricated in 1.2 ms. Each line is 375 μm long, ~1000 nm wide, and ~1000 nm high.

and that tryptophan, tyrosine, or histidine residues are advantageous for protein cross-linking.[21,25] The second possible mechanism occurs via a direct hydrogen abstraction from the protein molecule by the photoexcited initiator allowing for direct protein cross-linking.[22,25] This mechanism favors residues containing ketones, phenols, amines, or hydroquinones.[21,25] The possibility of inter- versus intramolecular reactions (i.e., actual cross-linking of proteins versus denaturation and precipitation) is addressed by Webster et al.[22] They provide evidence for intermolecular fibrinogen cross-linking under photoinitiation conditions similar to the method utilized here. In addition, it appears unlikely that simple precipitation is occurring since it is our experience that structures fabricated from proteins are stable for more than 1 month if kept hydrated. It seems unlikely that a simple precipitate would be stable over such a considerable storage time. Under our experimental conditions, cross-linking most likely occurs via the hydrogen abstraction mechanism as will be seen in the Efficiency of Fabrication section of the Results and Discussion.

Fabrication of Synthetic Structures. Our current experimental configuration utilizes a laser scanning microscope that is currently configured to only write lines and rectangles of various sizes. While this is a limitation compared to arbitrary writing or stage scanning capabilities, these simple shapes can lead to a wealth of interesting constructs. Figure 2 shows a SEM micrograph example of two lattice-like structures fabricated from a TMPTA, TEA (0.1 M), and 9F2C (1×10^{-4} M) solution. These were fabricated by creating a series of equally spaced parallel lines approximately 1 μm wide by 360 μm long, rotating the sample 45° or 90° and fabricating a second series of crossing lines. A closeup of crossing lines is shown at the bottom of the figure to verify the line width. Some fragmentation is apparent at the joints of two lines. This can be avoided by longer exposure to the laser light, hence building thicker, more robust structures. In these structures the light exposure was minimized to avoid polymerization reaction saturation and to improve feature resolution. The fabrication proceeds by the absorption ($\pi \rightarrow \pi^*$) of three photons of 780 nm light by the 9F2C. This absorption was verified by recording the absorption spectrum (not shown) of 9F2C and noting that it drops of sharply on either side of 780 nm, summing very closely to the known one-photon $\pi \rightarrow \pi^*$ transition at 260 nm. This three-photon transition cannot arise from the $n \rightarrow \pi^*$ transition which has a one-photon maximum at 330 nm. Although it is difficult to directly compare the efficiency of the two-photon polymerization using RB and three-photon using 9F2C, due to the unknown three-photon cross section of the latter, the absolute polymerization speed was relatively fast, where each line can be created in ~1.2 ms. Structures with such feature sizes may find applications in biomaterials and tissue engineering since they are at the subcellular biological scale.[7,26]

Three-dimensional rectangular features are also readily fabricated as demonstrated with polyurethane. Figure 3A shows microchannels fabricated by constructing a series of lines, with a height of ~1000 nm, the microscope stage (z) is then manually lowered by ~1000 nm, and a slab (360 μm × 200 μm × 1 μm) was fabricated on top of the lines. Optical microscopy demonstrates that the fabricated lines and the slab are in different focal planes, therefore indicating three-dimensionality. As our SEM does not provide sufficient tilting (90°) to provide an edge-on view, a cartoon of such a view is shown in Figure 3A. This structure exhibits the ability to create small fluidic channels with potential applications in microfluidics and "lab on a chip" type of devices. As another example of both chemistry and structure, Figure 3B shows a portion of a stepped pyramid (fabricated from TMPTA) with a second inverted stepped pyramid on top of the first, demonstrating the ability to construct overhanging features on relatively small scales, each layer being ~1 μm thick. A cartoon, to the right of the figure, provides an edge-on representation of the construct. The entire structure is not shown in the image since the goal was to present a clear picture of the overhanging features. The curved upper edge is an artifact of drying the sample for SEM. All of the corners did not curl, but due to the tilt limitations of our SEM, the corner shown here provides the best viewing opportunity. Similar structures are readily produced at scales that are a factor of 2−5 times smaller in the x and y directions. The three-dimensionality of this process and the expanded chemistry are two important improvements over standard lithographic and stamping techniques. Moreover, fabrication with our method can create structures quickly and in virtually any imaginable layout.

Fabrication of Proteinaceous Structures. A major goal of this work is to construct complex 3D structures from biopolymers. Figure 4A shows two stepped pyramids fabricated directly from a solution of BSA (1.5×10^{-4} M, 1% w/w) and rose bengal (1×10^{-4} M).

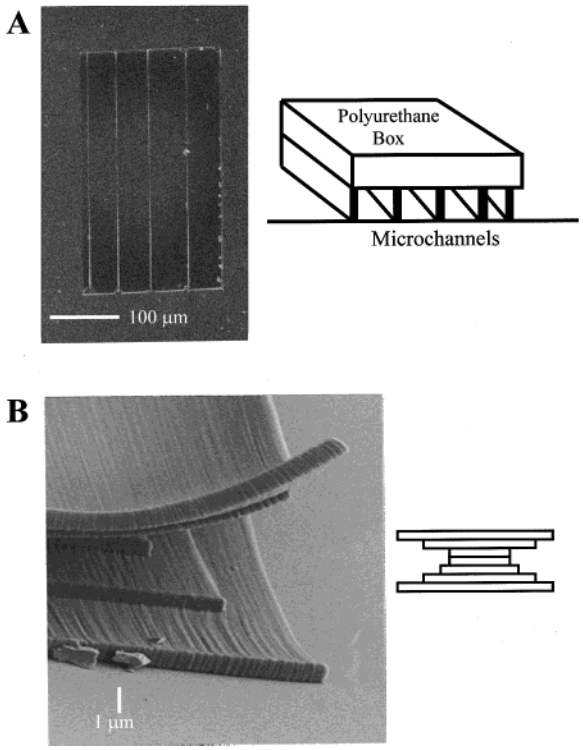

Figure 3. (A) An SEM micrograph of microchannels fabricated from polyurethane. The diagram depicts an edge-on view of the construct since we were unable to obtain sufficient tilt to image this view. Light microscopy shows significant different focal plains for the slab and the lines, suggesting that the structure has not collapsed. The lines are 375 μm long, ~1000 nm wide, and ~1000 nm high. (B) An SEM micrograph of a portion of a TMPTA structure which demonstrates the ability to construct overhanging features. The structure seen is a stepped pyramid with an inverted stepped pyramid placed on top of it. Each layer is less than 1000 nm in height. The curvature of the top few layers is an artifact of drying the sample for SEM. A diagram of an edge-on view of the entire construct is shown to the right of the image.

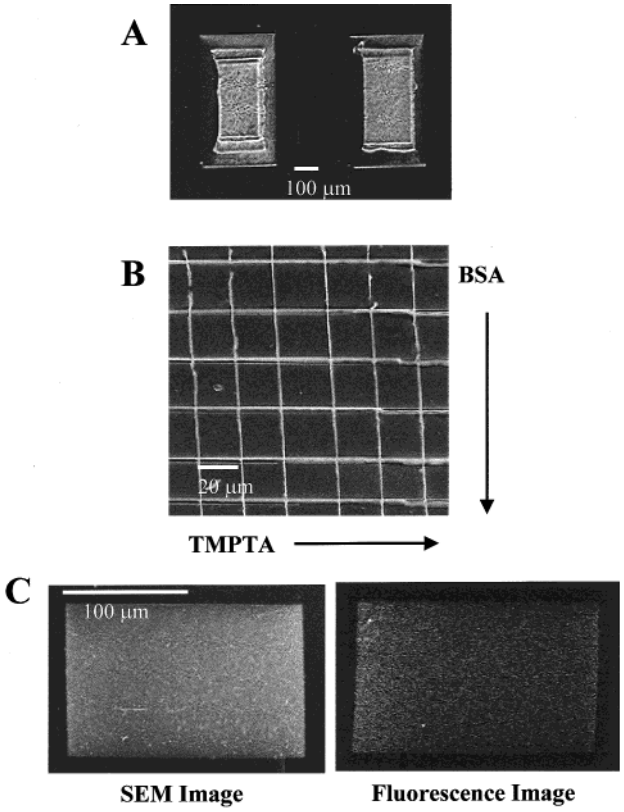

Figure 4. (A) Two BSA stepped pyramids, imaged with SEM, fabricated directly from a solution of BSA and RB. (B) A synthetic/protein hybrid lattice structure (imaged with SEM). The horizontal lines were fabricated first with TMPTA, and the vertical lines were then fabricated from BSA. See text for detailed description. (C) SEM and fluorescence image of a BSA construct fabricated in the presence of alkaline phosphatase, demonstrating the ability to entrap enzymes in matrixes, while maintaining activity; see text.

Fabrication rates with BSA are approximately 10-fold slower in comparison to the synthetic polymers. The 150 by 300 by 1 μm base layer requires approximately 10 s to fabricate. Subsequent layers require approximately a factor of 1.5−2 longer. These absolute times depend on the size of the construct, but the subsequent layers typically take longer than the base and slabs on top of a construct take longer to build than the identical size slab on the glass surface. The decrease in efficiency from the base layer to upper layers is presumably due to the loss of the glass/protein interaction that causes a greatly increased protein surface concentration in comparison to the bulk solution and hence improves local kinetics.[27] We can rule out enhancement from a glass surface reflection since only 4% of the incident radiation is reflected and the multiphoton absorption process scales with the photon density, making a reflection unlikely to cause significant cross-linking. To the best of our knowledge, this is the first example of two-photon optical freeform fabrication with proteins.

The ability to have multiple materials in a single construct has potential advantages where spatial control of chemistries is important; for example, spatially varying compositions can control biological interactions.[7] Hybrid constructs also makes it possible to control rates of release, material degradation, and other interactions with surrounding environments. Figure 4B shows an example of a two-constituent lattice-like structure where the horizontal lines are poly-TMPTA and the vertical lines are cross-linked BSA. To construct this structure, TMPTA was polymerized on the surface of a glass microscope slide. The sample was then washed (5 min) in acetone to remove any unpolymerized TMPTA and placed in a water bath for 10 min to exchange any acetone with water, and finally the water was exchanged with a 1.5×10^{-4} M BSA/1×10^{-4} M RB solution. This solution was exchanged several times to ensure that dilution did not occur. The sample was placed back on the microscope (~90° from the original position), and fabrication of the BSA lines was performed. Another hybrid matrix structure is seen in Figure 4C. Here the slab is fabricated in a solution containing BSA and alkaline phosphatase, resulting in a mixed biopolymer structure. Details describing this structure will be discussed in the following sections.

Obtainable Fabrication Resolution. The fabrication of both proteins and synthetic polymers using nonlinear photopolymerization provides a method of free-form fabrication that theoretically is capable of submicron resolution.[12] This resolution is determined by a number of factors including the optical point spread functions, absorption mechanisms, and the potential for reaction runaway. Here we compare minimum feature size using two- and three-photon excitation as a function of NA. Photoinitiation of TMPTA by RB or 9F2C requires the absorption of two or three photons, respectively, to initiate polymerization. While initiation at significantly different wavelengths would make for an

Table 1. Feature Size Objective Series (in nm)

	TMPTA		predicted resolution
numerical aperture (NA)	2-photon (rose bengal)	3-photon (9-fluorenone-2-carboxylic acid)	calcd Abbe limit at 800 nm excitation
0.5	2944	996	976
0.75	1191	606	650
1.3	735	344	375

unfair resolution comparison, RB and 9F2C were excited at similar wavelengths of 800 and 780 nm, respectively, affording a quantitative comparison.

Table 1 shows the experimental results for TMPTA polymerization along with the calculated one-photon point spread function. This point spread function is predicted by the Abbe relation:

$$d_{\min} = \frac{1.22\lambda}{2\mathrm{NA}} \quad (1)$$

where λ is the excitation wavelength used and d is the minimum spot size. Average laser powers were kept to a minimum to avoid extensive saturation effects. A minimum of 15 fabricated lines were measured at the ends and middle sections using SEM imaging, and the resulting measurements were averaged to obtain a typical feature resolution. These are shown in Table 1 for an excitation wavelength of 800 and 780 nm. It is clear that the TMPTA/RB reaction expands beyond the calculated resolution for all objectives used, presumably due to reaction runaway. Still, a general decrease in feature resolution is observed as would be predicted by eq 1.

9F2C photoinitiation of TMPTA provides finer feature resolution. This improvement in resolution is due to the higher required photon density for three-photon excitation resulting in a smaller point spread function relative to the two-photon case.[20] These experiments clearly show that this fabrication technique is capable of submicron resolution.

Efficiency of Fabrication. One of our fundamental questions concerning multiphoton free-form fabrication is the efficiency of polymerization or cross-linking of various monomers. It is important to have an understanding of this efficiency to optimize conditions for fabrication to determine the feasibility of practical manufacturing, as well as understand the limitations associated with this fabrication technique. Our first study of biopolymers efficiencies involves the cross-linking of BSA and fibrinogen as a function of rose bengal concentration. The concentration dependence is determined by measuring the number of line scans required to initiate visible fabrication. While polymerization or cross-linking may occur prior to becoming optically apparent, the same criteria are used for all experiments, thereby providing a relative self-consistent quantitative comparison. This observed polymerization or cross-linking was found to be reproducible over many trials and when new solutions or preparations were used.

Figure 5 shows the efficiency of cross-linking of BSA and fibrinogen as a function of rose bengal concentration versus the exposure dose (mJ/cm^2). It is found that the fibrinogen at low RB concentrations is ~2−10 times faster than BSA. This is presumably due to its much larger molecular weight of fibrinogen (340 kg/mol vs 66 kg/mol for BSA), giving rise to a larger volume protein

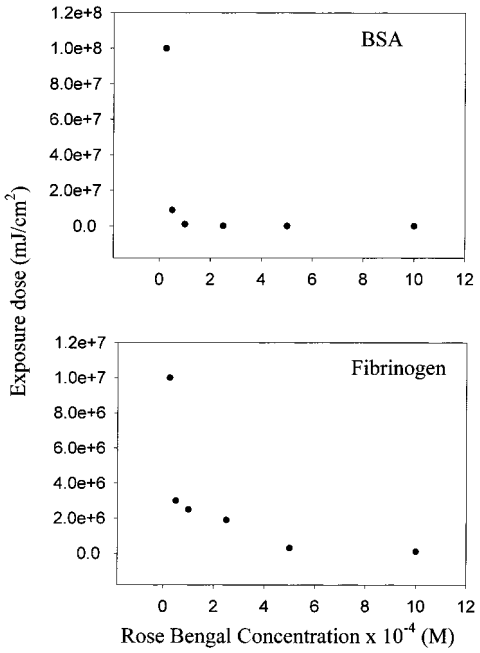

Figure 5. Upper graph shows the efficiency of polymerization of BSA as a function of rose bengal concentration. The lower graph shows the efficiency of polymerization of fibrinogen as a function of rose bengal concentration. Both show a marked dependency on rose bengal concentration, suggesting that the protein cross-linking mechanism is a direct hydrogen transfer from the protein to the photoexcited rose bengal. The minimum exposure time for optically apparent polymerization was recorded. This was done consistently and reproducibly between all experiments.

and many more potentially oxidizable amino acid residues. Hence, fewer cross-linking reactions and monomers are needed to reach optically detectable fabrication. This effect is lost when the concentration of RB is sufficiently high to negate the effects of photoactivator diffusion or fewer protein reactive sites. There is a marked dependence on the rose bengal concentration for both BSA and fibrinogen, suggesting that the mechanism leading to polymerization does not regenerate the dye. It has been suggested that one mechanism for protein cross-linking involves the reaction of singlet oxygen with a photooxidizable amino acid on the protein,[21,24,25] where singlet oxygen is produced upon energy transfer from the triplet state excited RB. After energy transfer to the molecular oxygen, the RB returns to the ground state and is still available for photoexcitation. Because of the RB concentration dependency, it is suggested that the dye is not regenerated and that the cross-linking of the proteins, in all probability, involves hydrogen transfer from the protein to the photoexcited dye. This presumably takes place at the ketone of the RB since triplet state ketones will abstract available hydrogen atoms and reduce to alcohols. This addition of a hydrogen atom to the rose bengal ketone destroys its ability to generate reactive long-lived triplet states and consequently destroys its ability to photoactivate polymerization or cross-link reactions. It is unlikely that the concentration dependence is due to photobleaching since it is well-known that multiphoton processes reduce photobleaching out of the focal plane,[17] and we have not observed any photobleaching of RB on the time scales used for fabrication. The hydrogen transfer mechanism seen here for both BSA and fibrinogen is consistent with a study done by Uhlich et al.[28] In their study BSA was photo-cross-linked with eosin

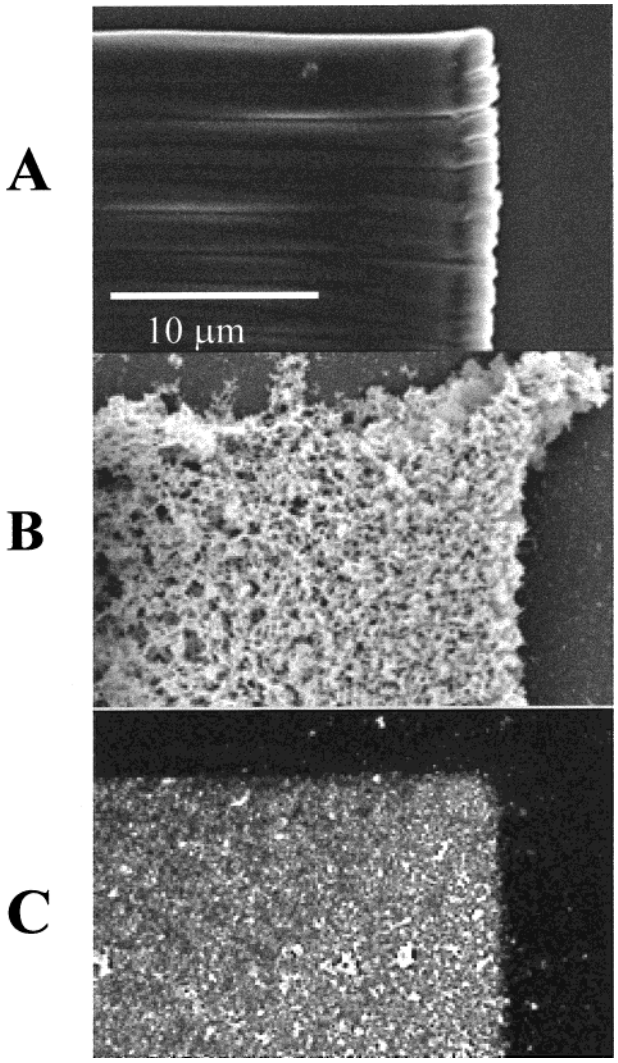

Figure 6. TMPTA (top), BSA (middle), and BSA/AP (bottom) SEM images demonstrating the change in surface texture as a function of fabrication material. All images are taken at 5000× magnification. See text for detailed description of process and implications.

Y while rigorously excluding molecular oxygen, suggesting that the dominate mechanism for protein photocross-linking does not follow the singlet oxygen pathway.

Surface Characteristics of Fabricated Structures. Scanning electron microscopy permits an analysis of the surface characteristics of the various fabricated materials. As seen in Figure 6, the surfaces of optically fabricated structures fall into one of three categories we will define here as low, medium, and highly textured. Both the polyurethane and TMPTA form low textured surfaces. All structures fabricated from these two monomers, analyzed using SEM, show little or no surface structure at 5000× magnification. As an example, Figure 6A shows the corner of a TMPTA slab. This low surface texture suggests that photopolymerization of these materials leads to uniform, densely packed polymer chains. The horizontal features seen in Figure 6A are a result of the line by line writing of the slab.

Protein cross-linking, by contrast, shows very different surface characteristics. Fabricated BSA and fibrinogen show a highly textured surface. An example of the BSA surface can be seen in Figure 6B. We suggest that this highly textured surface is a result of the significantly reduced cross-linking density compared to the synthetic example above.

When mixtures of proteins are fabricated, this can lead to different surface texture. Figure 6C shows a structure fabricated from a solution of BSA containing about 10% (w/w) alkaline phosphatase (AP). This mixed BSA and alkaline phosphatase structure forms a less textured surface (medium) than BSA alone, suggesting that the alkaline phosphatase is entrapped within the BSA. The change in texture is presumably a result of more efficient packing of two different size particles, as opposed to a monodispersed system. To test for a significant change in matrix porosity, we measured the relative time of release of 10 kDa dextran−tetramethylrhodamine (dextran−TMR) in the BSA/AP hybrid structure and the pure BSA structure. It was found that while the dextran releases from fabricated BSA structure within minutes, little or no release occurred over more than 90 min from the hybrid BSA/AP structure. This ability to tailor the textures or porosity of structures will be critical to the development of devices with different controllable release characteristics. Similarly, porosity and surface texture are of paramount concern in tissue engineering scaffolds and other bioengineering applications.

Diffusion. Hydrogel and protein matrixes have often been used as drug delivery devices or sustained release devices.[29−31] The ability to fabricate with both hydrogel materials and various proteins at the milli-, micro-, and nanometer scale expands the scope of such devices beyond the relatively large millimeter scale of devices available today. Critical to creating useful release devices is the entrapment of large molecular weight compounds that act as model systems for biomolecules or pharmaceutics. Optical fabrication from solution provides a convenient method for entrapping molecules in a chosen matrix by simply including the molecule in the fabrication solution. As an example, a solution of BSA (1.5×10^{-4} M), rose bengal (2.5×10^{-4} M), and alkaline phosphatase (7×10^{-5} M) was used as the fabrication media. The fabrication was performed on a BSA adsorbed glass microscope slide, minimizing the nonspecific adsorption of the AP to the glass substrate. Two-photon fabrication of a solid slab ($\sim 200\ \mu m \times 110\ \mu m \times 1\ \mu m$) took place at an excitation wavelength of 808 nm. This slab was then washed in a distilled water bath (~4500× dilution factor) for 15 min. The fabricated structure was then returned to the microscope, and a solution of ELF-97 phosphatase substrate was added. This phosphatase substrate is soluble in water, but upon reaction with AP, a phosphate group is cleaved, and the product becomes insoluble and thereby precipitates in the immediate vicinity of the enzyme. Additionally, upon phosphate cleavage, the ELF-97 phosphatase substrate emission changes from diffuse, dim blue to a punctate, bright yellow-green fluorescence. Figure 4C shows a fluorescence image of this simple slab at 5 min after the addition of the ELF-97 phosphatase substrate. A strong fluorescence is observed in the fabricated zone, indicating that the phosphate cleavage reaction has occurred. Since the precipitation of the ELF-97 phosphatase substrate was very fast, it was not possible to perform a time series fluorescence study. However, at time zero no fluorescence was observed, and after 10 min optical sectioning of the slab shows penetration of the substrate throughout the BSA matrix. This observed

fluorescence is only possible if the AP is incorporated throughout the BSA matrix. It is also apparent that the AP does not lose its activity upon entrapment in photo-cross-linked BSA. This retention in activity upon cross-linking is attributed to the fact that the active site is probably small compared to the entire enzyme and thus remains unaffected.

The BSA/AP matrix shows that mixed proteins structures may be readily fabricated from solution. For a functional release device that is a solid matrix like many well-known hydrogel delivery devices,[29−31] fabrication should entrap and not cross-link a species of interest. This ability was used to design a model system for sustained release of a macromolecule. Using BSA to form the entrapping matrix, fabrication is performed in a solution also containing 10 or 40 kDa dextran−TMR (0.1 and 0.03 M, respectively). Fabrication of structures in this solution will presumably entrap the fluorescently labeled sugar but not covalently link the sugar to the protein. This is assumed to be the case since hydrogen abstraction seems more favorable from an amino acid side chain than from a sugar. It is noted that fabrication of a BSA matrix in the presence of the large dextran−TMR may effect pore size, density, and other physical properties of the matrix. Our goal here is not to quantify these effects but rather demonstrate that fabrication is possible, that the sugars are indeed entrapped, and that simple diffusion will occur from these small constructs. Additional studies are underway that load the species of interest after fabrication in order to examine the effects of their presence on fabrication and diffusion. If the fabrication does not involve covalent bonding to the dextrans, the rate of diffusion of the dextrans out of the BSA matrix can then be monitored by recording the integrated fluorescence intensity as a function of time. Diffusion out of a matrix can be interpreted via the random motion of solute molecules and Fick's second law.[32] Thermodynamically the concentration gradient is positive, so the flux will be in the direction of decreasing concentration, i.e., out of the matrix.

We monitored the release of both dextran−TMRs from identical size slabs with varying degrees of cross-linking density. Varying the time of fabrication by scanning multiple rasters in the same fabrication zone was used to control this density, where longer exposure times result in higher cross-link density. At this time we do not have a way of directly monitoring cross-link density; therefore, we report the exposure dose (mJ/cm^2) as a measure of relative densities. After fabrication, the structure is washed for 3 min in flowing distilled water in order to remove any excess solution that would interfere with the fluorescence of the BSA/dextran matrix. Since this washing will initiate diffusion of the dextrans out of the fabricated structure, wash times were kept as short as possible, but sufficiently long to provide for adequate rinsing. Figure 7 plots the averaged (four or more experiments) normalized fluorescence intensity as a function of diffusion time for the 10 and 40 kDa dextran−TMR. The exposure dose is shown next to each plot. Laser exposure time, for fluorescence measurements, for each point is kept at a minimum to reduce any chance of photobleaching. Complementary images recorded at much longer laser exposure times show little to no photobleaching, so it is assumed that the decay in fluorescence is not significantly effected by photobleaching. The solid lines in Figure 7 are an exponential fit to the data. The half-life of the 10 kDa

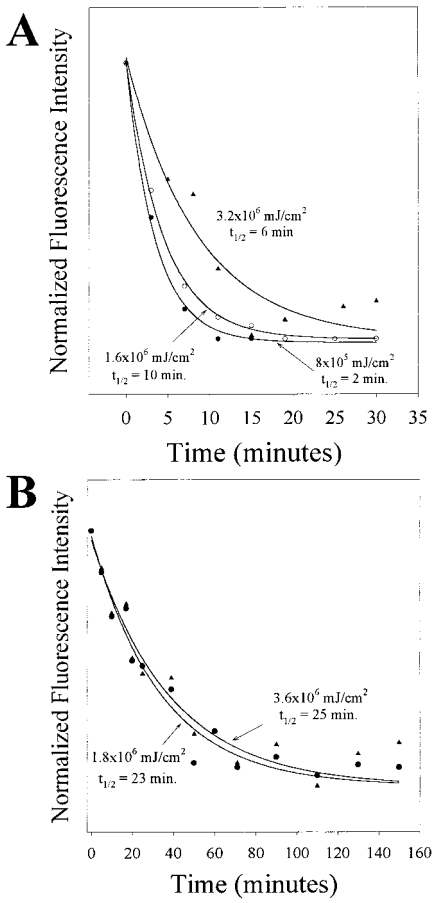

Figure 7. (A) Rate of release of 10 kDa dextran−TMR from a BSA matrix as measured by loss of fluorescence. The exposure dose is shown in mJ/cm^2 and denotes the relative level of cross-linking in the construct. Filled circles denote an exposure dose of 8×10^5 mJ/cm^2, open circles denote an exposure dose of 1.6×10^6 mJ/cm^2, and triangles denote an exposure dose of 3.2×10^6 mJ/cm^2. The solid lines are a single-exponential fit to the data. (B) Rate of release of 40 kDa dextran−TMR from a BSA matrix. The exposure dose is shown in mJ/cm^2 and denotes the level of cross-linking in the construct. Filled circles denote an exposure dose of 1.8×10^6 mJ/cm^2, and triangles denote an exposure dose of 3.6×10^6 mJ/cm^2.

dextran−TMR, for an exposure dose of 8×10^5, 1.6×10^6, and 3.2×10^6 mJ/cm^2, is 2, 3, and 6 min, respectively, and the half-life for the 40 kDa dextran−TMR for an exposure dose of 1.8×10^6 and 3.6×10^6 mJ/cm^2 is 23 and 25 min, respectively. The diffusion coefficient for each BSA slabs can be calculated from the half-life via the equation[33]

$$D = (0.0492L^2)/t_{1/2} \qquad (2)$$

where $t_{1/2}$ is the half-life and L is the slab thickness, which is assumed to be 1 μm. The calculated diffusion coefficients for the various BSA slabs are show in Table 2.

As would be expected, the dextrans' diffusion half-life increases as the matrix density (i.e., exposure dose) increases. For a purely matrix diffusion-limited process, the time should scale with the cubed root of the mass of the diffusing species, assuming similar shape and constant density of the solute.[32−34] Noting the times of the 10 and 40 kDa dextran−TMR diffusion, it is apparent that this is not the case. A dramatic increase in the half-life is seen, suggesting that the different molecular

Table 2. Calculated Diffusion Coefficients

BSA−10 kDa dextran	exposure dose (mJ/cm^2)	8×10^5	1.6×10^6	3.2×10^6
	half-life (min)	2	3	6
	D (μm^2/min)	0.02	0.016	0.008
BSA−40 kDa dextran	exposure dose (mJ/cm^2)	1.8×10^6	3.6×10^6	
	half-life (min)	23	25	
	D (μm^2/min)	0.002	0.002	
acrylamide−R610	exposure dose (mJ/cm^2)	1.8×10^7	2.7×10^7	
	half-life (min)	9	31	
	D (μm^2/min)	0.0055	0.0016	

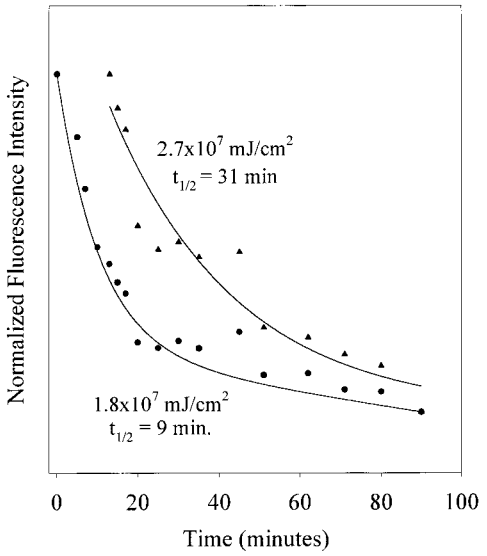

Figure 8. Rate of release of rhodamine 610 from an acrylamide matrix as a function of relative cross-link density (i.e., exposure dose (mJ/cm^2)). Filled circles denote an exposure dose of 1.8×10^7 mJ/cm^2, and triangles denote an exposure dose of 2.7×10^7 mJ/cm^2.

weight sugars do indeed effect matrix density. This is a serious implication for the construction of release devices, as a detailed understanding of constituent effects on the fabrication of gel and protein matrices is required to make reliable and predictable devices. Therefore, future experiments are planned to provide insight into the question of matrix/solute interaction.

It is also possible to model drug delivery from synthetic microstructures. Acrylamide slabs were fabricated in the presence of rhodamine 610 (R610). Rhodamine 610 has a molecular weight (479 g/mol) that approximates the molecular weight of many drugs. R610 was also used since its two-photon absorption maximum is near 830 nm, which has minimal absorption overlap with rose bengal. This red-shifted excitation maximum allows for the monitoring of the R610 emission with little or no rose bengal fluorescence background. Figure 8 is the average normalized diffusion curves for the acrylamide/R610 diffusion at an exposure dose of 1.8×10^7 and 2.7×10^7 mJ/cm^2, with each curve determined from an average of four or more trials. The solid lines represent an exponential fit to the data, yielding a half-life of 9 and 31 min for an exposure dose of 1.8×10^7 and 2.7×10^7 mJ/cm^2, respectively. Calculated diffusion coefficients for acrylamide−R610 are shown in Table 2. A marked decrease in the rate of release of the R610 is observed for only a modest increase in exposure dose. The diffusion rate of water-soluble species, out of a thin slab of hydrogel, into an infinite aqueous bath has been derived by Crank.[33]

$$\frac{M_t}{M_\infty} = \frac{4}{\sqrt{\pi}}\left[\frac{Dt}{L^2}\right]^{1/2} \tag{3}$$

where D is the diffusion coefficient of the solute and M_t and M_∞ are the amount of solute released in time t and the total amount of solute released, respectively. Crank's equation for diffusion shows that the fractional release is proportional to the square root of the time and is accurate for the first 60% of release. While these data do deviate from a square root of time relation, it does show a close trend, suggesting that the release of R610 from the acrylamide matrix is close to being diffusion limited. These results demonstrate the ability to entrap a drug-sized molecule and have it release from a hydrogel at a controllable rate. To extend this rate to longer times will require increased matrix density and concentration of the entrapped species.

Conclusion

We have presented several examples of structures fabricated using a new method of nonlinear optical free-form nanofabrication that is capable of photopolymerizing both synthetic and biopolymeric materials as well as synthetic/protein hybrids and protein/enzyme hybrids on the submicron scale. The rates of polymerization of both bovine serum albumin and fibrinogen have been determined. SEM was used to show that the surface texture depends on the fabrication material. Entrapment of molecular species into a fabricated matrix was demonstrated by cross-linking AP in BSA, entrapping polysaccharides in BSA and entrapping rhodamine 610 in polyacrylamide. The entrapped compounds were studied as sustained release systems modeling macromolecule and drug release, respectively. Our current studies are examining the entrapment of bioactive compounds that diffuse from a polymer matrix and stand to control cell growth and morphology.

Acknowledgment. S.L.G. and J.D.P. gratefully acknowledge support from a University of Connecticut Health Center Faculty Research Grant, the NIH (HL55451) and the Patrick and Catherine Weldon Donaghue Medical Research Foundation. P.J.C. gratefully acknowledges support from NSF Academic Research Infrastructure DBI-9601609 and the State of Connecticut Critical Technology program. The authors also thank Victoria L. Scranton for her insightful conversations and technical support.

References and Notes

(1) Service, R.; Amato, I. *Science* **1998**, *282*, 396−405. Burns, M. A.; Johnson, B. N.; Brahmasandra, S. N.; Handique, K.; Webster, J. R.; Krishnan, M.; Sammarco, T. S.; Man, P. M.; Jones, D.; Heldsinger, D.; Mastrangelo, C. H.; Burke, D. T. *Science* **1998**, *282*, 484−487. Weigl, B. H.; Yager, P. *Science* **1999** 283, 346−347.

(2) Chen C. S.; Mrksich, M.; Huang, S.; Whitesides, G. M.; Ingber, D. E. *Biotechnol. Prog.* **1998**, *14*, 356−363.

(3) Xia, Y.; Whitesides, G. M. *Langmuir* **1997**, *13*, 2059−2067.
(4) Jackman, R. J.; Brittain, S. T.; Adams, A.; Prentiss, M. G.; Whitesides, G. M. *Science* **1998**, *280*, 2089−2091. Jackman, R. J.; Brittain, S. T.; Adams, A.; Wu, H.; Prentiss, M. G.; Whitesides, S.; Whitesides, G. M. *Langmuir* **1999**, *15*, 826−836. Woolley, T.; Sensabaugh, G. F.; Mathies, R. A. *Anal. Chem.* **1997**, *69*, 2181−2186.
(5) James, C. D.; Davis, R. C.; Kam, L.; Craighead; H. G.; Isaacson, M.; Turner, J. N.; Shain, W. *Langmuir* **1998**, *14*, 741−744. St. John, P. M.; Davis, R.; Cady, N.; Czajka, J.; Batt, C. A.; Craighead, H. G. *Anal. Chem.* **1998**, *70*, 1108−1111.
(6) Nealey, P. F.; Black, A. J.; Wilbur, J. L.; Whitesides, G. M. *Molecular Electronics*; Jortner, J., Ratner, M., Eds.; IUPAC: Oxford, England, 1997; pp 343−367.
(7) Pitts, J. D.; Campagnola, P. J.; Goodman, S. L. Trans. Sixth World Biomaterials Congress, Kamuela, HI, May 15−20, No. 611, in press.
(8) Maruo, S.; Nakamura, O.; Kawata, S. *Opt. Lett.* **1997**, *22*, 132−134.
(9) Witzgall, G.; Vrijen, R.; Yablonovitch, E. *Opt. Lett.* **1998**, *23*, 1745−1747.
(10) Cumpston, B. H.; Ananthavel, S. P.; Barlow, S.; Dyer, D. L.; Ehrlich, J. E.; Erskine, L. L.; Heikal, A. A.; Kuenler, S. M.; Lee, I.-Y. S.; McCord-Maughon, D.; Qin, J.; Rockel, H.; Rumi, M.; Wu, X.-L.; Marder, S. R.; Perry, J. W. *Nature* **1999**, *398*, 51−54.
(11) Campagnola, P. J.; DelGuidice, D.; Epling, G.; Hoffacker, K. D.; Howell, A. R.; Pitts, J. D.; Goodman, S. L. *Macromolecules* **2000**, *33*, 1511−1513.
(12) Goppert-Mayer, M. *Ann. Phys.* **1931**, *9*, 273−275.
(13) Eaton, D. F. *Adv. Photochem.* **1986**, *13*, 427−487.
(14) Mishra, M. K.; Yagci, Y. *Handbook of Radical Vinyl Polymerization*; Marcel Dekker: New York, 1998; pp 149−201.
(15) Chen, C. S. H *J. Polym. Sci., Part A* **1965**, *3*, 1107−1125.
(16) Oster, G. *Nature* **1954**, *173*, 300−301.
(17) Denk, W.; Piston, D. W.; Webb, W. W. *Handbook of Biological Confocal Microscopy*; Pawley, J. B., Ed.; Plenum Press: New York, 1995; pp 445−458.
(18) Goodman, S. L. *Handbook of Biomaterials Evaluation*, 2nd ed.; von Recum, A. F., Ed.; Taylor and Francis: Philadelphia, PA, 1999; pp 613−629.
(19) Jager, W. F.; Lungu, A.; Chen, D. Y.; Neckers, D. C. *Macromolecules* **1997**, *30*, 780−791. Egerton, P. L.; Pitts, E.; Reiser, A. *Macromolecules* **1981**, *14*, 95−100. Egerton, P. L.; Trigg, J.; Hyde, E. M.; Reiser, A. *Macromolecules* **1981**, *14*, 100−104. Reiser, A.; Egerton, P. L. *Macromolecules* **1979**, *12*, 670−673.
(20) Gu M. R.; Sheppard, C. J. *J. Microsc.* **1995**, *177*, 128−137.
(21) Foote, C. S. *Free Radicals in Biology;* Pryor, W. A., Ed.; Academic Press: New York, 1976; Vol. 2, pp 85−134.
(22) Webster, A.; Britton, D.; Apap-Bologna, A.; Kemp, G. *Anal. Biochem.* **1989**, *179*, 154−157.
(23) Verweij, H.; Dubbelman, T. M. A. R.; Van Steveninck, J. *Biochim. Biophys. Acta* **1981**, *647*, 87−94.
(24) Shen, H.-R.; Spikes, J. D.; Kopecekova, P.; Jopecek, J. *J. Photochem. Photobiol. B: Biol.* **1996**, *34*, 203−212. Shen, H.-R.; Spikes, J. D.; Kopecekova, P.; Jopecek, J. *J. Photochem. Photobiol. B: Biol.* **1996**, *34*, 213−219.
(25) Balasubramanian, D.; Du, X.; Zigler Jr., J. S. *Photochem. Photobiol.* **1990**, *52*, 761−768.
(26) Flemming, R. G.; Murphy, C. J.; Abrams, G. A.; Goodman, S. L.; Nealey, P. F. *Biomaterials* **1999**, *20*, 573−588.
(27) Ratner, B. D.; Hoffman, A. S.; Schoen, F. J.; Lemons, J. E. *Biomaterials Science;* Academic Press: San Diego, CA, 1996; pp 136−140. Cooper, S. L.; Peppas, N. A. *Biomaterials: Interfacial Phenomena and Applications*; ACS Advances in Chemistry Series; American Chemical Society: Washington, DC, 1982; pp 233−244.
(28) Uhlich, T.; Hubbell, J. A. 23rd Annual Meeting of the Society for Biomaterials Transcripts, Society for Biomaterials, New Orleans, LA, April 30−May 4 1997, p 104.
(29) Ulbrich, K.; Subr, V.; Seymour, L. W.; Duncan, R. *J. Controlled Release* **1993**, *24*, 181−190.
(30) Zignani, M.; Tabatabay, C.; Gurny, R. *Adv. Drug Delivery Rev.* **1995**, *16*, 51−60.
(31) West, J. L.; Hubbell, J. A. *React. Polym.* **1995**, *25*, 139−147.
(32) Burnette, R. R. In *Controlled Drug Delivery, Fundamentals and Applications*, 2nd ed.; Robinson, J. R., Lee, V. H., Eds.; Marcel Dekker: New York, 1987; Chapter 2.
(33) Crank, J. *The Mathematics of Diffusion*, 2nd ed.; Oxford University Press: London, UK, 1975.
(34) Baker, R. W.; Lonsdale, H. K. In *Controlled Release of Biologically Acive Agents*; Tanquary, A. C., Lacey, R. E., Eds.; Plenum Press: New York, 1974.

MA9910437